ChemElectroChem

Supporting Information

Simultaneously Incorporating Atomically Dispersed Co-N_x Sites with Graphitic Carbon Layer-Wrapped Co_9S_8 Nanoparticles for Oxygen Reduction in Acidic Electrolyte

Jun Wu, Mengjun Gong, Wuyi Zhang, Asad Mehmood, Jinfeng Zhang, Ghulam Ali, and Anthony Kucernak*

1. High resolution TEM images and EDS mapping of the Co SACs and Co SACs + Co_9S_8 catalysts.

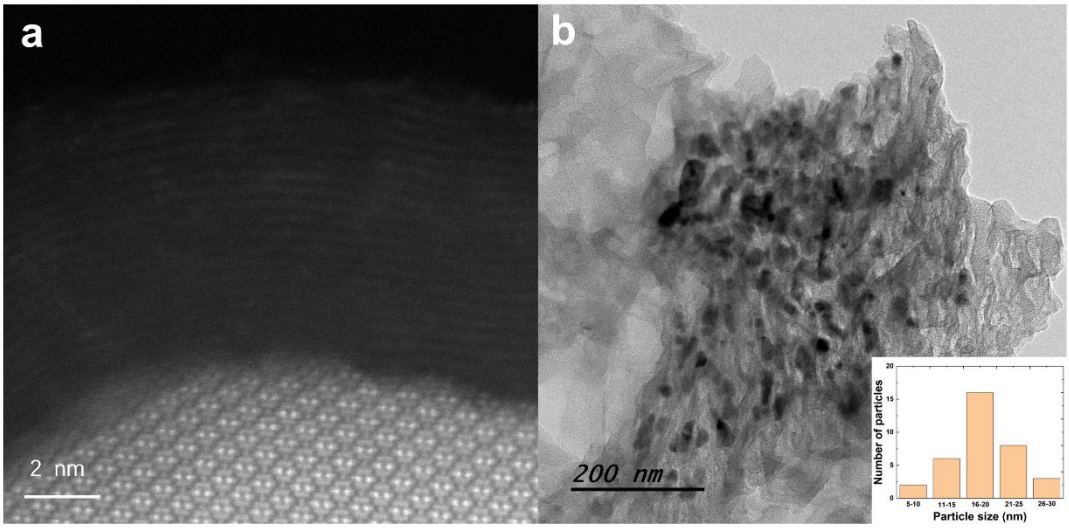

Figure S1 (a) HAADF-STEM image of Co SACs + Co_9S_8 catalyst. (b) size distribution of Co_9S_8 nanoparticles.

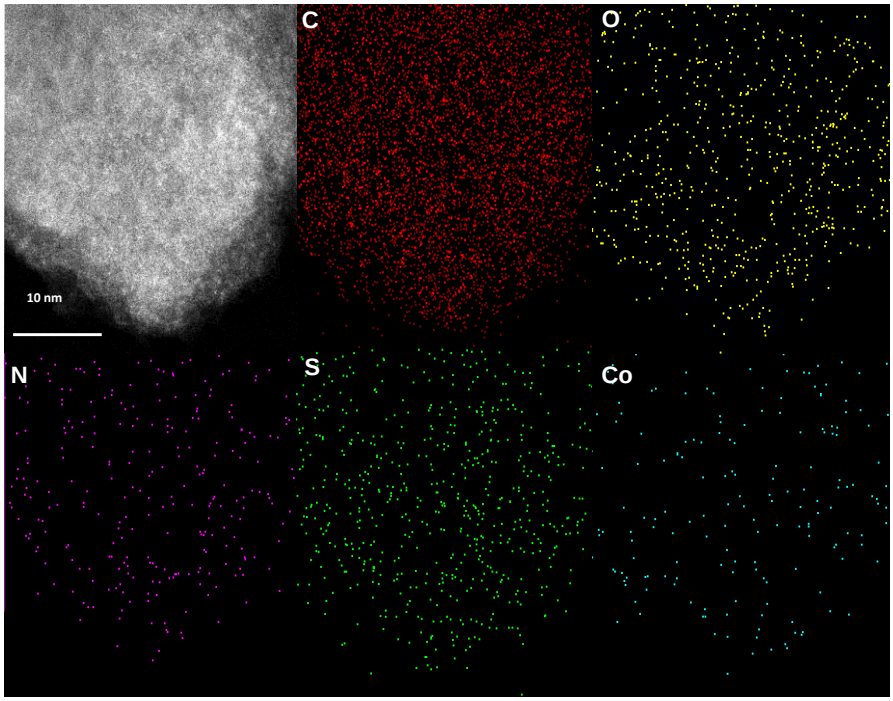

Figure S2 EDS mapping of the Co SACs + Co_9S_8 catalyst.

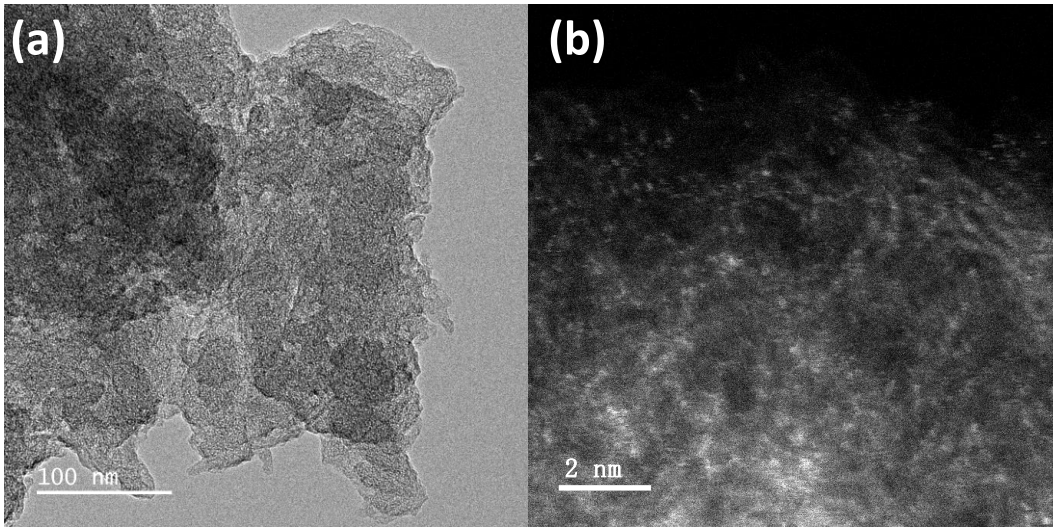

Figure S3 (a) HRTEM image and (b) HAADF-STEM image of the Co SACs catalyst.

2. Raman spectra in lower wavenumber range of the Co SACs and Co SACs + Co_9S_8 catalysts.

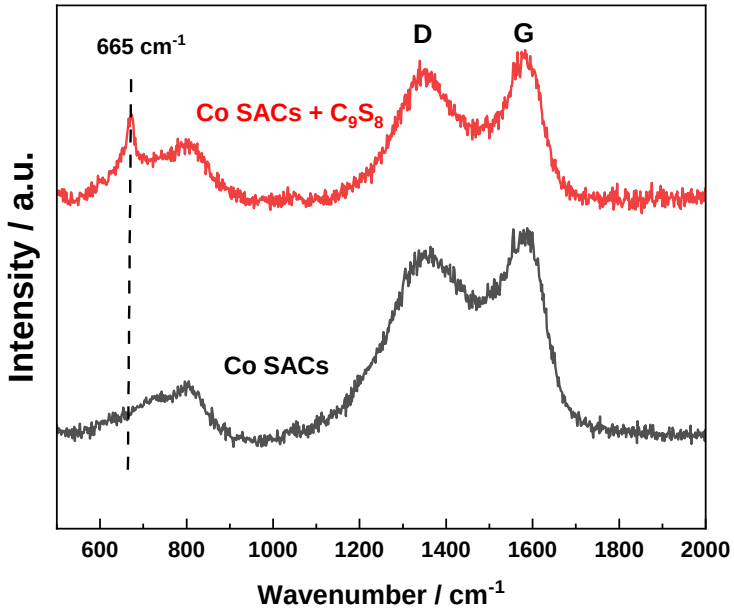

Figure S4 Raman spectra of the Co SACs and Co SACs + Co_9S_8 catalysts.

3. Table S1: External, microporous, and total surface area of the Co SACs and Co SACs + Co_9S_8 catalysts determined by N_2 adsorption.

Catalyst	External SA [m^2g^{-1}]	Microporous SA [m^2g^{-1}]	Total SA [m^2g^{-1}]
Co SACs	91.7	228.3	320
Co SACs + Co_9S_8	70.6	338.6	409.2

Table S2: Average pore size and pore volume of the Co SACs and Co SACs + Co_9S_8 catalysts determined by N_2 adsorption.

Catalyst	Average pore size [nm]	Pore volume [cm^3g^{-1}]
Co SACs	5.85	0.46
Co SACs + Co_9S_8	4.11	0.51

4. XPS survey spectra, S 2p and Co 2p spectra of the Co SACs and Co SACs + Co_9S_8 catalysts

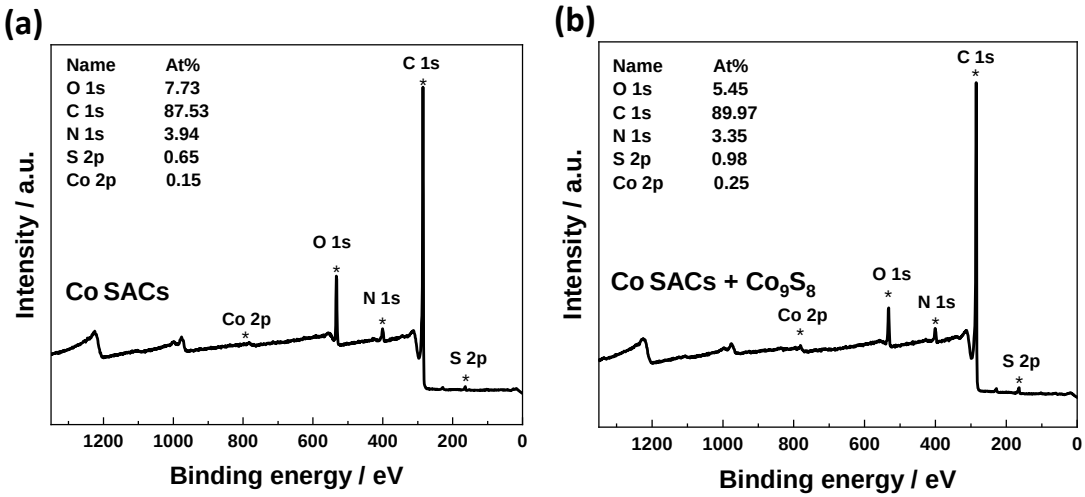

Figure S5 XPS survey spectrum of (a) Co SACs and (b) Co SACs + Co_9S_8 catalyst.

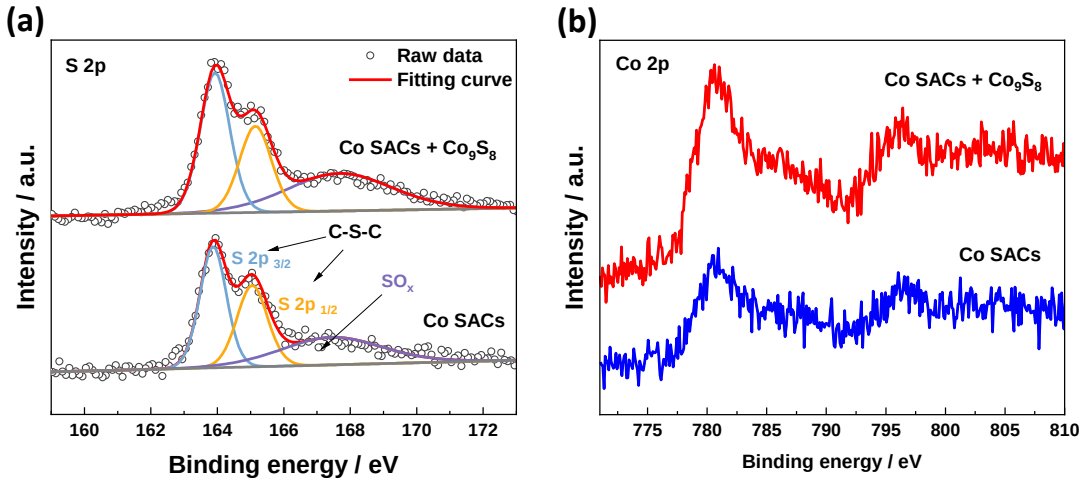

Figure S6 High-resolution (a) S 2p and (b) Co 2p XPS spectra of the Co SACs and Co SACs + Co_9S_8 catalysts.

5. EXAFS fitting results of the Co SACs and Co SACs + Co_9S_8 catalyst

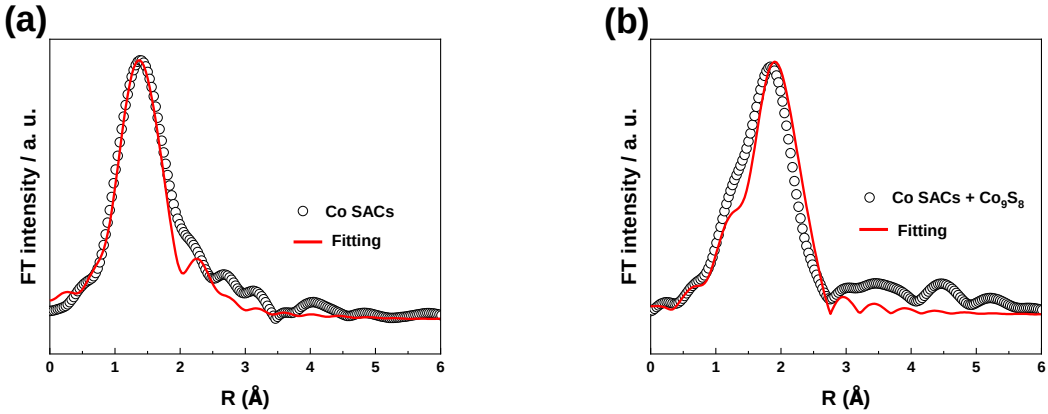

Figure S7 The EXAFS fitting curves of the (a) Co SACs and (b) Co SACs + Co_9S_8.

Table S3 Co K-edge EXAFS curve fitting parameters for the Co SACs and Co SACs + Co_9S_8

Sample	Bond type	Coordination number	Bond length (Å)	Bond disorder σ^2 (Å^2)	R factor
Co SACs	Co-N	2.1	1.88	0.0067	0.003
	Co-C	1	2.15	0.0007	
Co SACs + Co_9S_8	Co-N	2.8	1.89	0.016	0.008
	Co-S	0.85	2.22	0.007	
	Co-Co	3.6	2.49	0.005	

6. Steady-state RRDE measurements investigating the 2nd heat treatment effect on the Co SACs and Co SACs + Co_9S_8 catalysts

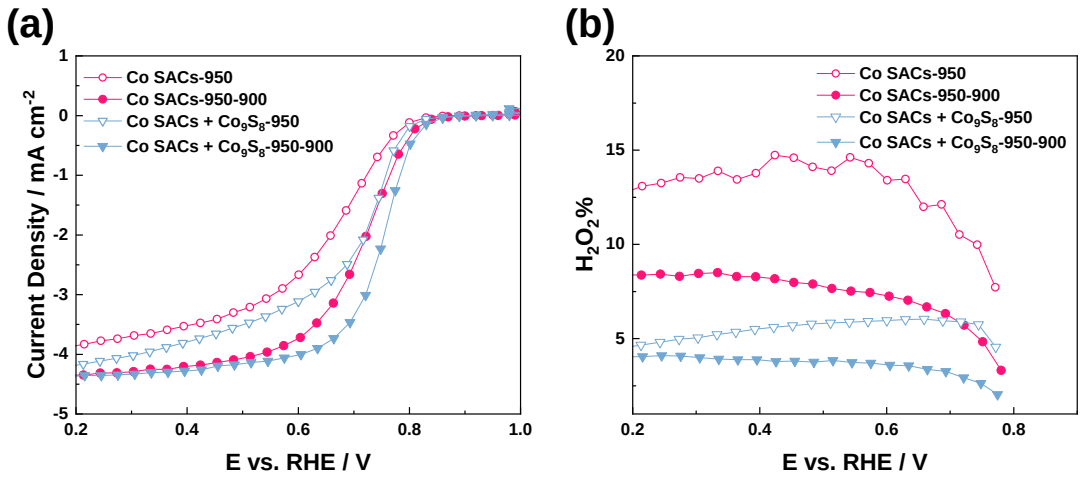

Figure S8 Steady-state RRDE measurements of the Co SACs and Co SACs + Co_9S_8 catalysts in O_2-saturated 0.5 M H_2SO_4 after the first and second heat treatment, catalyst loading: 750μg cm^{-2}, rotating speed: 1600 rpm, 30 mV step potential, 30s hold.

7. Co 2p, N 1s, and S 2p XPS spectra of the Co SACs and Co SACs + Co_9S_8 catalysts after the first and second heat treatment

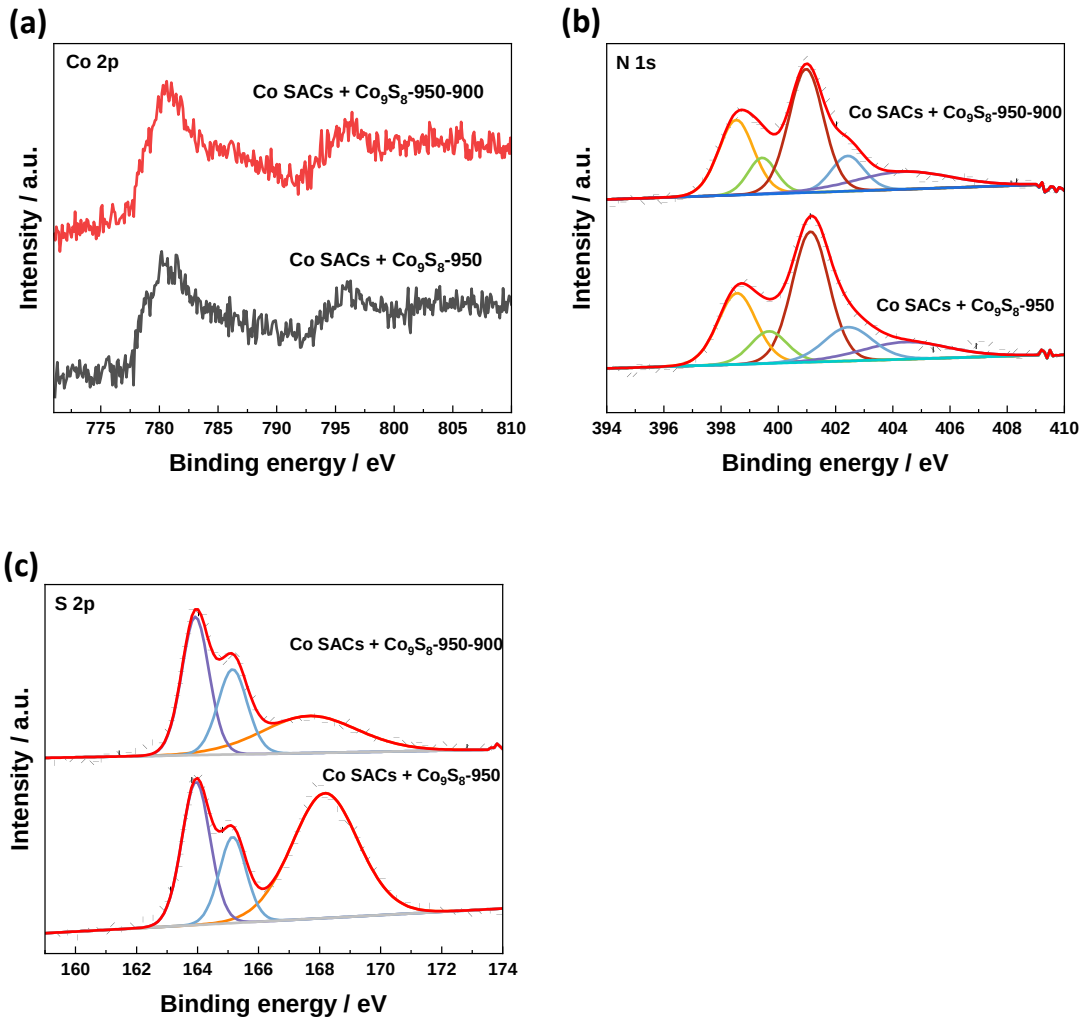

Figure S9 High resolution (a) Co 2p, (b) N 1s, and (c) S 2p XPS spectra of the Co SACs and Co SACs + Co_9S_8 catalysts after first and second heat treatment

8. Table S4: Surface elemental composition of the best acid performing catalysts before and after the second heat treatment as detected by XPS

Catalysts	C [at%]	N [at%]	O [at%]	S [at%]	Metal [at%]
Co SACs-950	86.78	3.97	7.85	1.34	0.06
Co SACs-950-900	87.53	3.94	7.73	0.65	0.15
Co SACs+Co_9S_8-950	87.32	3.38	7.23	1.98	0.09
Co SACs+Co_9S_8-950-900	89.97	3.35	5.45	0.98	0.25

9. Long term chronoamperometry test on the Co SACs + Co_9S_8 catalyst.

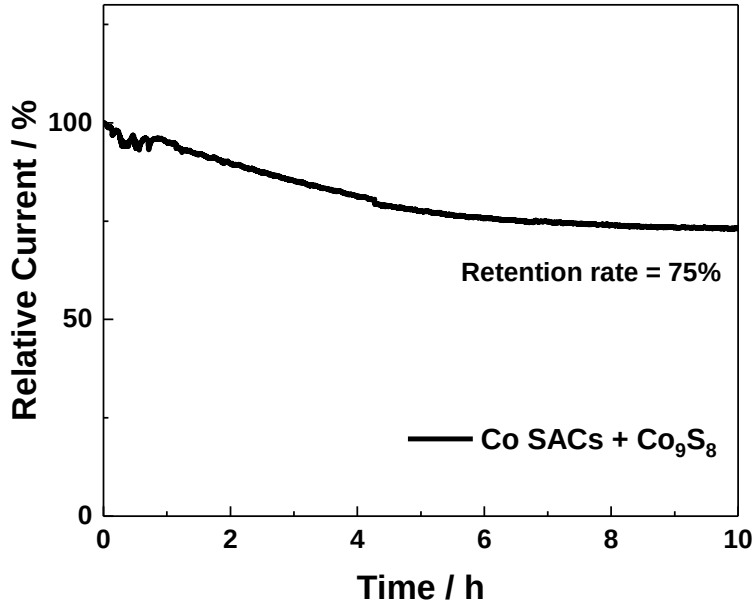

Figure S10 Chronoamperometry responses (in O_2-saturated 0.5 M H_2SO_4) of Co SACs + Co_9S_8 catalysts coated carbon paper, catalysts loading: 1mg cm^{-2}.

10. Physical characterization on the post-ORR test Co SACs + Co_9S_8 catalyst

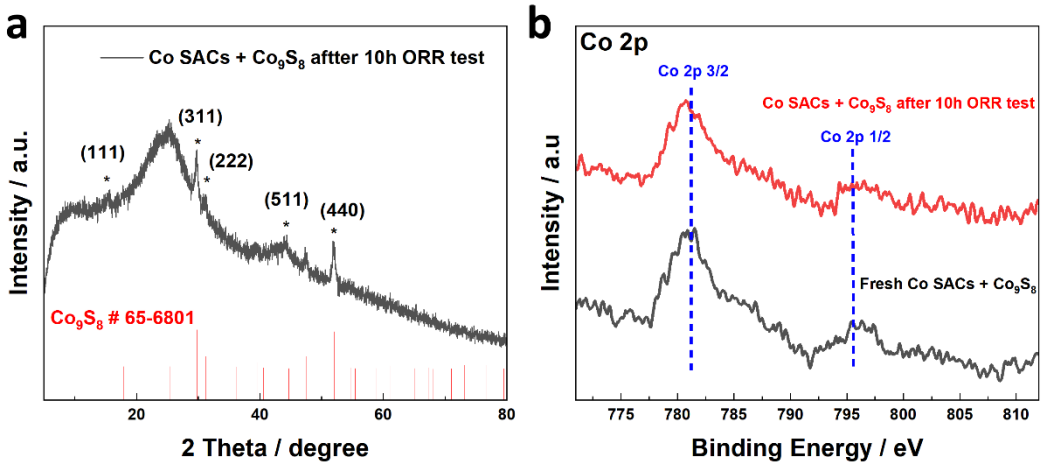

Figure S11 (a) XRD pattern and (b) Co 2p region XPS spectra of Co SACs + Co_9S_8 catalysts after 10h ORR tests.

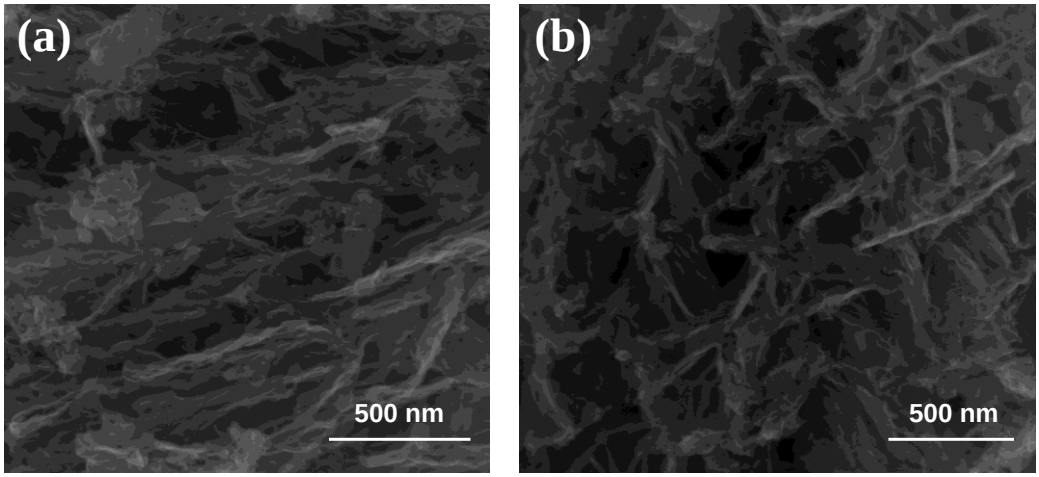

Figure S12 SEM images of the fresh Co SACs + Co_9S_8 catalysts and after 10h ORR tests.

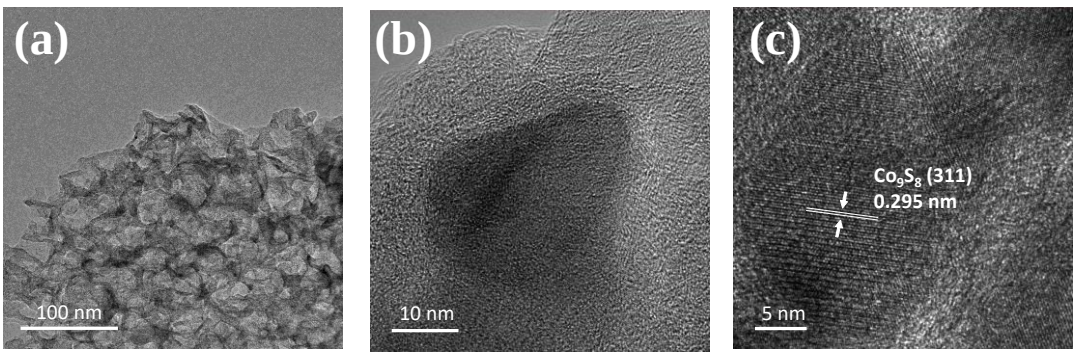

Figure S13 TEM images of the fresh Co SACs + Co_9S_8 catalysts and after 10h ORR tests.

11. RRDE nitrite poisoning experiments on the Co SACs and Co SACs + Co_9S_8 catalysts.

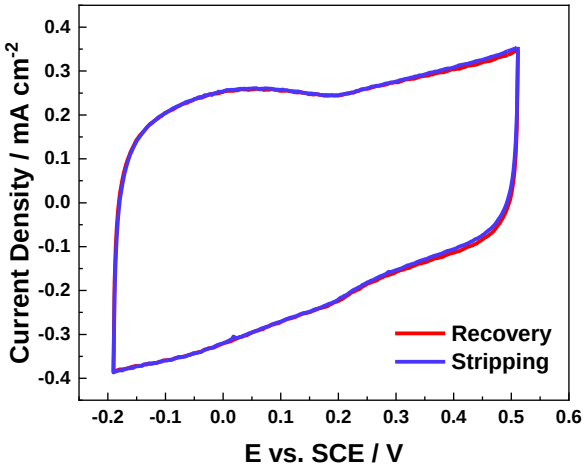

Figure S14 wide range baseline scan (avoid nitrite reduction area) for the catalyst layer before, during and after nitrite adsorption. All experiments were performed in a 0.5 M acetate buffer at pH 5.2 for the Co SACs + Co_9S_8 catalyst using a rotating disk electrode setup; catalyst loading: 0.2mg cm^{-2}.

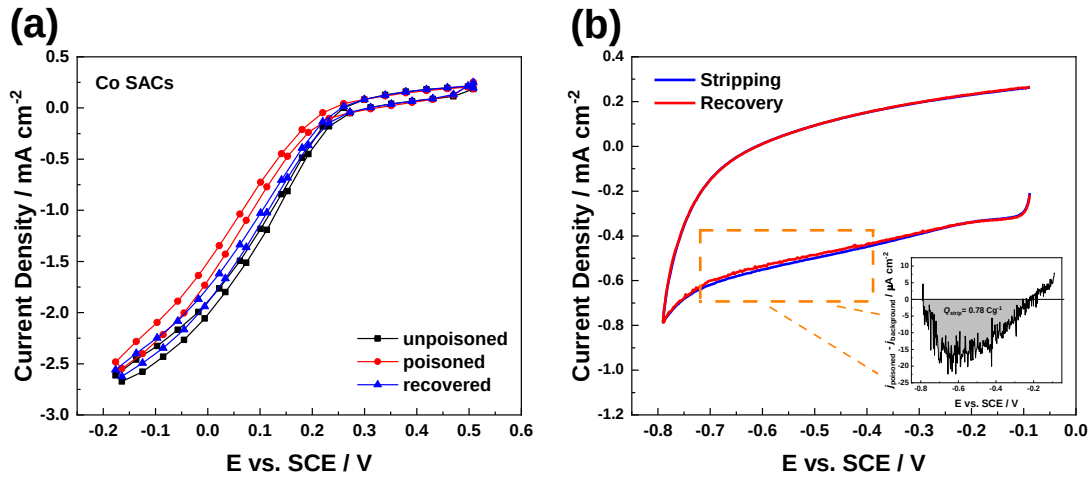

Figure S15 (a) Steady state ORR tests of catalyst layer before, during and after nitrite adsorption. (b) Narrow baseline scan in the nitrite reductive stripping region during and after nitrite adsorption. Inset is the stripping charge calculated by subtracting the recovered from poisoned curve in Figure S15b. All experiments were performed in a 0.5 M acetate buffer at pH 5.2 for the bare Co SACs catalyst using a rotating disk electrode setup; catalyst loading: 0.2 mg cm^{-2}.

12. Physical characterizations on the Co SACs + high loading Co_9S_8 catalyst.

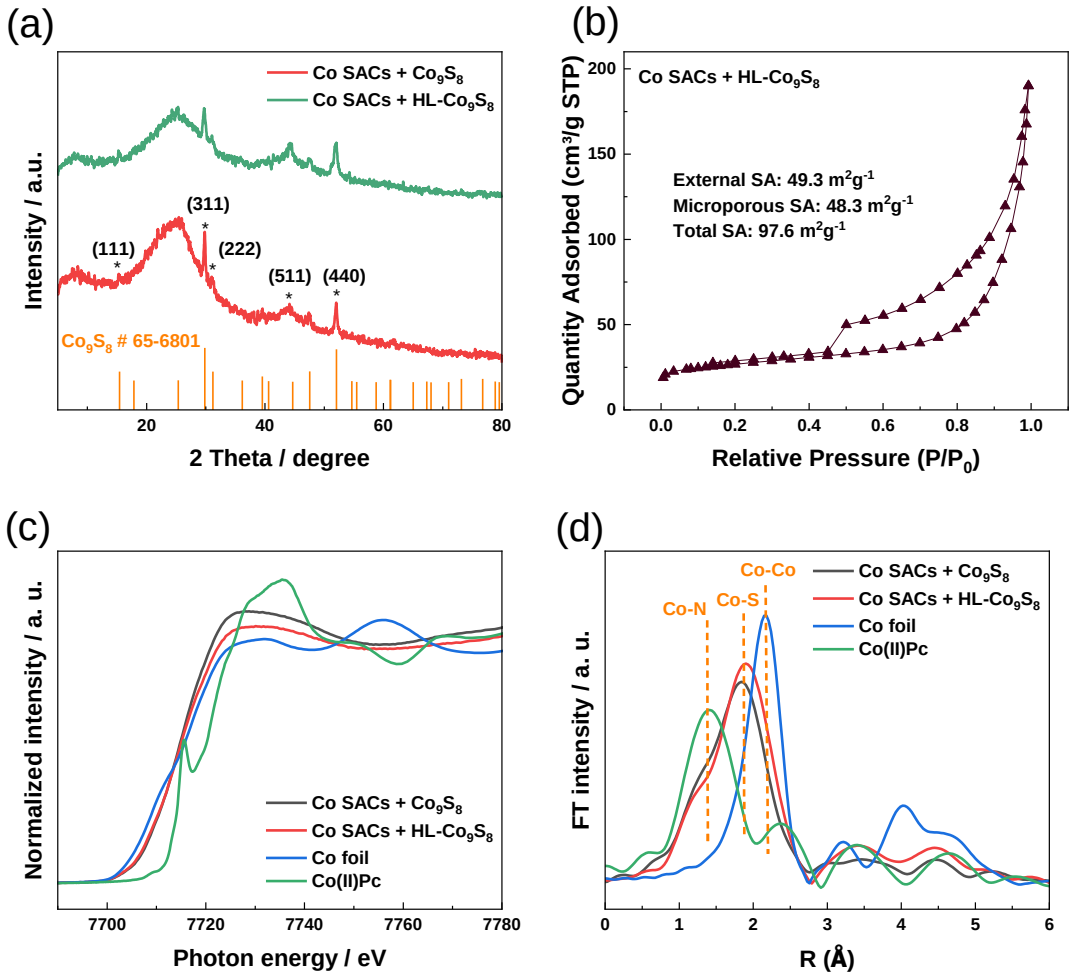

Figure S16 (a) XRD patterns of the Co SACs + Co_9S_8 and Co SACs with high loading Co_9S_8 catalysts. (b) N_2 isotherms of the Co SACs with high loading Co_9S_8 catalysts. (c) Co K-edge XANES spectra and (d) Fourier transforms of k^2-weighted Co-K-edge EXAFS spectra of the Co SACs + Co_9S_8 and Co SACs with high loading Co_9S_8 catalysts, and the references samples.

13. EXAFS fitting results of the Co SACs + HL-Co_9S_8 catalyst

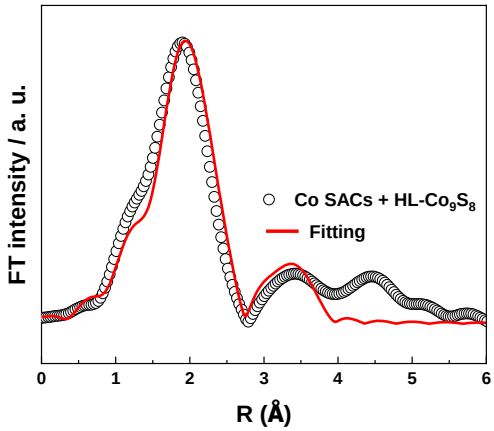

Figure S17 The EXAFS fitting curves of the Co SACs + HL Co_9S_8.

Table S5 Co K-edge EXAFS curve fitting parameters for the Co SACs + HL Co_9S_8.

Sample	Bond type	Coordination number	Bond length (Å)	Bond disorder σ^2 ($Å^2$)	R factor
Co SACs + HL Co_9S_8	Co-N	2.56	1.89	0.016	0.008
	Co-S	1	2.22	0.007	
	Co-Co_1	3.66	2.49	0.005	
	Co-S-Co_2	1.2	3.63	0.002	

14. Steady-state ORR polarizations on the Co SACs + high loading Co_9S_8 catalyst.

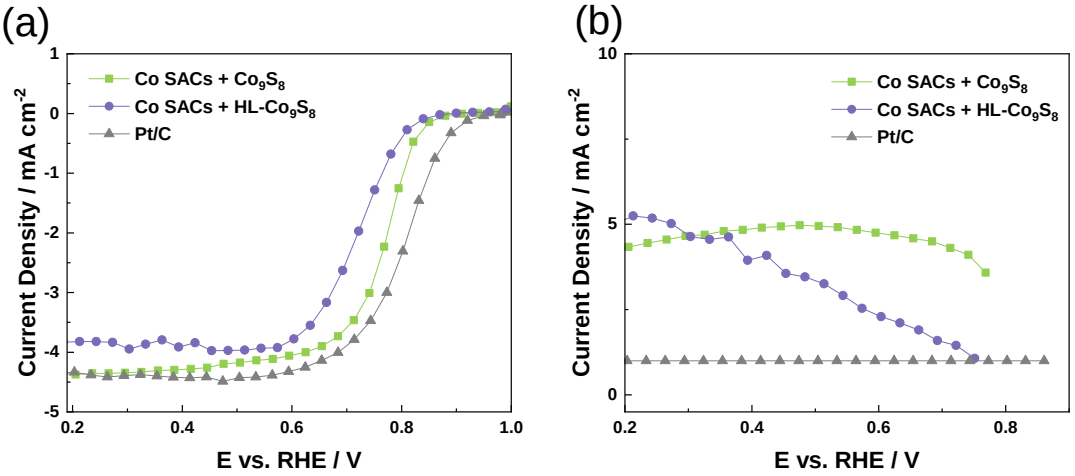

Figure S18 (a) Steady-state RRDE measurements of the Co SACs + Co_9S_8 and Co SACs with high loading Co_9S_8 catalysts in O_2-saturated H_2SO_4, catalysts loading: 750μg cm^{-2}, rotating speed: 1600 rpm, 30 mV step potential, 30s hold.

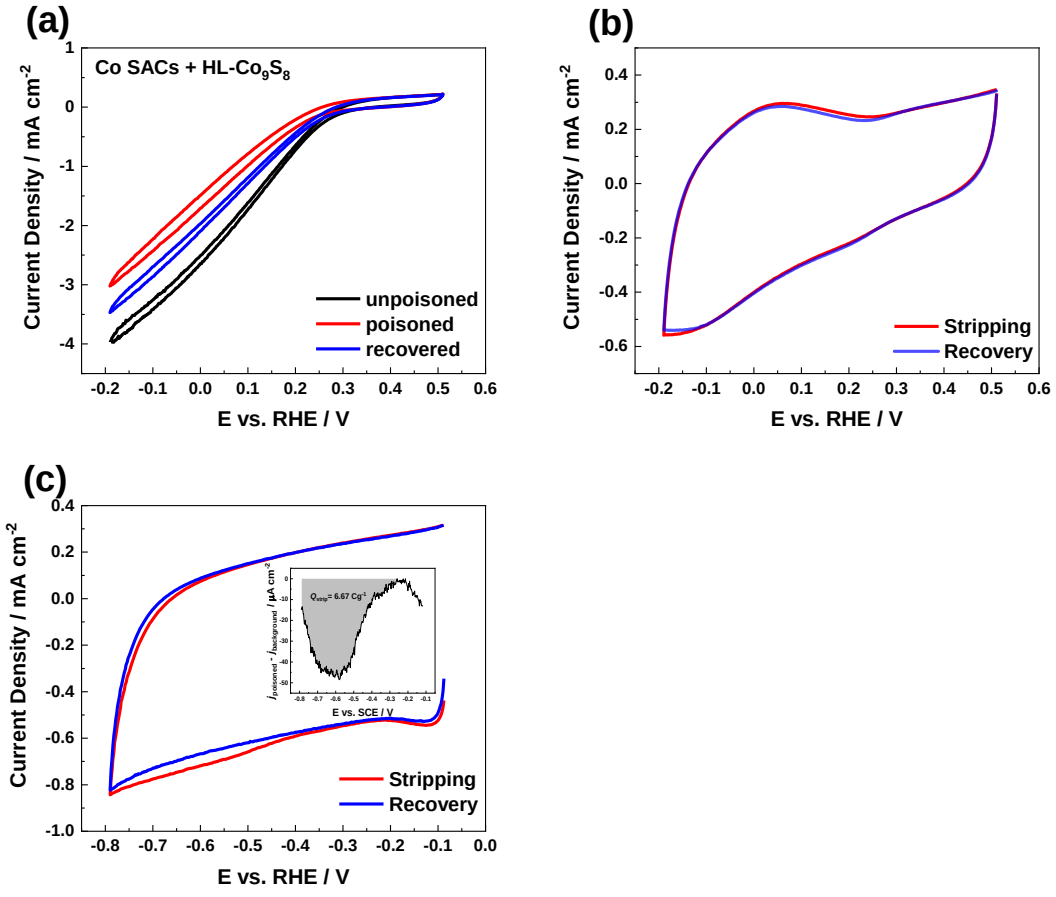

Figure S19 (a) Steady state ORR tests of catalyst layer before, during and after nitrite adsorption. (b) Wide range baseline scan (avoid nitrite reduction area) for the catalyst layer during and after nitrite adsorption. (c) Narrow baseline scan in the nitrite reductive stripping region during and after

nitrite adsorption. Inset is the stripping charge calculated by subtracting the recovered from poisoned curve in Figure S19c. All experiments were performed in a 0.5 M acetate buffer at pH 5.2 for the bare Co SACs catalyst using a rotating disk electrode setup; catalyst loading: 0.2 mg cm^{-2}.

15. Comparison of H_2-O_2 PEMFC performance of the highest performing Co SACs + Co_9S_8 catalyst with other reported non-Fe PGM-free catalysts

Table S6: Comparison of H_2-O_2 PEMFC performance of the highest performing Co SACs + Co_9S_8 catalyst with other reported non-Fe PGM-free catalysts

Catalysts	Catalyst loading [mg cm^{-2}]	Back pressure [bar]	P_{max} [W cm^{-2}]
3wt%-Co-N_x/C	4.0	2.0	0.61
CoNC@KL600[1]	4.0	1.0	0.72
Co (mlm)-NC (1.0)[2]	6.3	1.0	0.64
H@CoNC[3]	3	1.5[a]	0.66
d-(Co_{NP}/Co_{SA}-N-C)[4]	4	2.0	1.207
Co-N-C@F127[5]	4	1.0	0.87
1.6%CoNC-$ArNH_3$[6]	3	2.0	0.8

[a] 22 psi

16. Comparison of H_2-Air PEMFC performance of the highest performing Co SACs + Co_9S_8 catalyst with other reported non-Fe PGM-free catalysts

Table S7: Comparison of H_2-Air PEMFC performance of the highest performing Co SACs + Co_9S_8 catalyst with other reported non-Fe PGM-free catalysts

Catalysts	Catalyst loading [mg cm^{-2}]	Back pressure [bar]	P_{max} [W cm^{-2}]
3wt%-Co-N_x/C	4.0	2.0 bar	0.25
Co (mlm)-NC (1.0)[2]	6.3	1.0 bar	0.32
d-(Co_{NP}/Co_{SA}-N-C)[4]	4.0	1.0 bar	0.454
Co-N-C@F127[5]	4.0	1.0 bar	0.27
20Co-NC-1100[7]	4.0	2.1 bar[a]	0.28
Co-N-PCNF[8]	4.0	1.0 bar	0.4
1.6%CoNC-ArNH_3[6]	3	2.0 bar	0.305

[a] 30 psi

Reference

1. Wang, R.; Zhang, P.; Wang, Y.; Wang, Y.; Zaghib, K.; Zhou, Z., ZIF-derived Co–N–C ORR catalyst with high performance in proton exchange membrane fuel cells. *Progress in Natural Science: Materials International* **2020,** *30* (6), 855-860.
2. Xie, X.; He, C.; Li, B.; He, Y.; Cullen, D. A.; Wegener, E. C.; Kropf, A. J.; Martinez, U.; Cheng, Y.; Engelhard, M. H., Performance enhancement and degradation mechanism identification of a single-atom Co–N–C catalyst for proton exchange membrane fuel cells. *Nature Catalysis* **2020,** *3* (12), 1044-1054.
3. Liu, J.; Wan, X.; Liu, S.; Liu, X.; Zheng, L.; Yu, R.; Shui, J., Hydrogen Passivation of M–N–C (M= Fe, Co) Catalysts for Storage Stability and ORR Activity Improvements. *Advanced Materials* **2021,** *33* (38), 2103600.
4. Cheng, X.; Yang, J.; Yan, W.; Han, Y.; Qu, X.; Yin, S.; Chen, C.; Ji, R.; Li, Y.; Li, G., Nano-geometric deformation and synergistic Co nanoparticles—Co-N 4 composite sites for proton exchange membrane fuel cells. *Energy & Environmental Science* **2021,** *14* (11), 5958-5967.
5. He, Y.; Hwang, S.; Cullen, D. A.; Uddin, M. A.; Langhorst, L.; Li, B.; Karakalos, S.; Kropf, A. J.; Wegener, E. C.; Sokolowski, J., Highly active atomically dispersed CoN 4 fuel cell cathode catalysts derived from surfactant-assisted MOFs: carbon-shell confinement strategy. *Energy & Environmental Science* **2019,** *12* (1), 250-260.
6. Chen, L.; Liu, X.; Zheng, L.; Li, Y.; Guo, X.; Wan, X.; Liu, Q.; Shang, J.; Shui, J., Insights into the role of active site density in the fuel cell performance of Co-NC catalysts. *Applied Catalysis B: Environmental* **2019,** *256*, 117849.
7. Wang, X. X.; Cullen, D. A.; Pan, Y. T.; Hwang, S.; Wang, M.; Feng, Z.; Wang, J.; Engelhard, M. H.; Zhang, H.; He, Y., Nitrogen-coordinated single cobalt atom catalysts for oxygen reduction in proton exchange membrane fuel cells. *Advanced Materials* **2018,** *30* (11), 1706758.
8. He, Y.; Guo, H.; Hwang, S.; Yang, X.; He, Z.; Braaten, J.; Karakalos, S.; Shan, W.; Wang, M.; Zhou, H., Single cobalt sites dispersed in hierarchically porous nanofiber networks for durable and high-power PGM-free cathodes in fuel cells. *Advanced Materials* **2020,** *32* (46), 2003577.